optica

Rotational quantum beat lasing without inversion: supplementary material

MARIA RICHTER[1,*,**], MARIANNA LYTOVA[2,5,**], FELIPE MORALES[1], STEFAN HAESSLER[3], OLGA SMIRNOVA[1,4], MICHAEL SPANNER[2,5], AND MISHA IVANOV[1,6,7]

[1] Max-Born-Institute, Max-Born Straße 2A, 12489 Berlin, Germany
[2] Department of Physics, University of Ottawa, Ottawa K1N 6N5, Canada
[3] Laboratoire d'Optique Appliquée, CNRS, École Polytechnique, ENSTA Paris, Institut Polytechnique de Paris, 181 Chemin de la Hunière et des Joncherettes, 91120 Palaiseau, France
[4] Technische Universität Berlin, Straße des 17. Juni 135, 10623 Berlin, Germany
[5] National Research Council of Canada, 100 Sussex Drive, Ottawa K1A 0R6, Canada
[6] Department of Physics, Humboldt University, Newtonstraße 15, 12489 Berlin, Germany
[7] Blackett Laboratory, Imperial College London, SW7 2AZ London, UK
[*] Corresponding author: maria.richter@mbi-berlin.de
[**] These authors contributed equally.

Published 27 May 2020

This document provides supplementary information to "Rotational quantum beat lasing without inversion," https://doi.org/10.1364/OPTICA.390665. It provides details on the theoretical modeling of the light amplification process around the 391 nm line in N_2^+ for laser pulse intensities typical in laser filamentation experiments. The model accounts for laser-induced alignment of the neutral N_2 molecule, its alignment-dependent strong-field ionization into the laser-dressed states of the molecular ion, and the full laser-induced electronic, vibrational and rotational dynamics in the ion involving the ground and first two excited states. Amplification is studied applying conventional transient absorption theory, revealing the link between light-induced ionization and alignment dynamics in molecules and the possibility of light amplification without population inversion.

1. LASER-INDUCED DYNAMICS IN THE NEUTRAL

We consider a short pump pulse with a full width at half maximum (FWHM) of $\simeq 23$ fs in intensity, which aligns and ionizes neutral N_2, and subsequently drives the electronic, vibrational and rotational dynamics in the ion.

We assume an initial thermal ensemble of neutral nitrogen molecules at approximately room temperature ($T \simeq 298$ K), including initial angular momenta up to $J_{0,\max} = 30$.

The effect of laser-induced alignment of the neutral molecule with the pump laser polarization direction is described in the impulsive regime [1], where the short pulse adds the phase

$$\Phi_N(\theta; t_{\rm ion}) = -\frac{1}{4}\,\Delta\alpha\cos^2\theta\,F_{0,\rm pu}^2\int_{-\infty}^{t_{\rm ion}} f_{\rm pu}^2(t)\,dt \qquad \text{(S1)}$$

to the molecular wave function. Here, $\Delta\alpha = 4.349$ a.u. is the polarizability anisotropy of the neutral molecule, θ the angle between the molecular axis and the electric field vector of the pump pulse, $F_{0,\rm pu}$ is the peak electric field strength, $t_{\rm ion}$ the time of ionization, and $f_{\rm pu}(t)$ the $\sin^2$-envelope of the pump pulse:

$$f_{\rm pu}(t) = \begin{cases} \sin^2\left(\frac{\pi t}{T_{\rm pu}}\right) & ,0 \le t \le T_{\rm pu} \\ 0 & ,\text{else} \end{cases} \qquad \text{(S2)}$$

where $T_{\rm pu}$ is the duration of the pump pulse. For the peak intensities considered in this work, we assume ionization to take place at the peak of the laser pulse envelope, i.e., $t_{\rm ion} = T_{\rm pu}/2$.

2. STRONG-FIELD IONIZATION OF N_2 AND THE ROLE OF RECOLLISION

Our model includes strong-field ionization from the ground state of N_2 into the ground ($X\,^2\Sigma_g^+$; denoted by X below) and

second excited ($B\,^2\Sigma_u^+$; denoted by B below) electronic states of N_2^+.

Ionization is described using the angle-dependent ionization rate $w(\theta)$ calculated with the method developed in Refs. [2, 3]. It employs *ab initio* quantum chemistry multielectron wave functions for the neutral and cation states, calculated using the GAMESS-US electronic structure code [4]. The wave function of the continuum electron associated with each ionic state is represented on a three-dimensional Cartesian numerical grid. Using a reflection-free absorbing potential [5] at the grid edges, ionization yields are obtained by monitoring the liberated electron density absorbed at the grid boundaries.

Typically smaller grids are used for calculation of ionization probabilities alone, where the outgoing flux of the continuum electron wave function is absorbed almost immediately after being liberated. However, varying the size of the simulation box allows us to gauge the role of excitation of the parent ion in the X state via recollision with the liberated electron. Varying the edge of the absorbing boundary from 10 a.u. to 45 a.u., we find no considerable change in the X- and B state ionization yield, concluding that recollision of the photoelectron with the parent ion plays a negligible role. As a consequence, for considering processes taking place in the ion, the photoelectron can be integrated out. Here, the electron-ion entanglement is important. Since the X and B states have opposite parity, the photoelectron wave packets originating from each state will also carry opposite parity. Therefore, integrating over the photoelectron wave packets after the pump has passed, destroys the coherence between the X and B states that could have been produced during strong-field ionization.

We set the ionization ratio between X and B to $r_X/r_B = 1.0/0.2$ (see Eq. (S8) below), however, our results do not depend on this ratio sensitively. For the pump pulse parameters and temperature used in Figs. 1 and 2 of the main article, the onset of net gain is found at the ratio $r_x/r_B \simeq 1.0/0.1$.

3. LASER-INDUCED DYNAMICS IN THE ION

To account for the effects of the electric field on the ionic states populated by the pump, we prepare the ion in the polarized (field-dressed) states. For that purpose, we initialize the laser-ion interaction with a smooth ramp-up of the pump field over 1.5 cycles (≈ 4 fs) from zero to the corresponding field strength at time of ionization, $F_{0,\mathrm{pu}}(t_{\mathrm{ion}})$, see Fig. S1. This way, we avoid shake-up effects associated with the preparation of wave packets on the field-free ionic states while the laser field is strong, which may lead to spurious excitations of the A and B states of the ion. Instead, the wave packets placed on the field-free ionic states are smoothly transferred into the wave packets on the dressed states.

From the time of ionization until the end of the pump pulse, we describe the laser-driven electronic, vibrational and rotational wave packet dynamics in N_2^+ in the impulsive alignment regime. We first expand the wave function in a superposition of vibronic eigenstates, where $a_{n\nu}^{(n_0\nu_0)}$ and $E_{n\nu}$ indicate the amplitude and eigenenergy of the vibrational level ν, with $\nu = 0,\ldots,9$, and electronic state n, with $n = X, A, B$, corresponding to the three energetically lowest states of N_2^+: $X\,^2\Sigma_g^+$, $A\,^2\Pi_u$, and $B\,^2\Sigma_u^+$.

The vibronic eigenfunctions and eigenenergies, $\psi_{n\nu}$ and $E_{n\nu}$, are obtained by solving the eigenvalue equation,

$$\left[-\frac{1}{2\mu}\frac{\partial^2}{\partial R^2} + E_n(R)\right]\psi_{n\nu} = E_{n\nu}\psi_{n\nu}, \tag{S3}$$

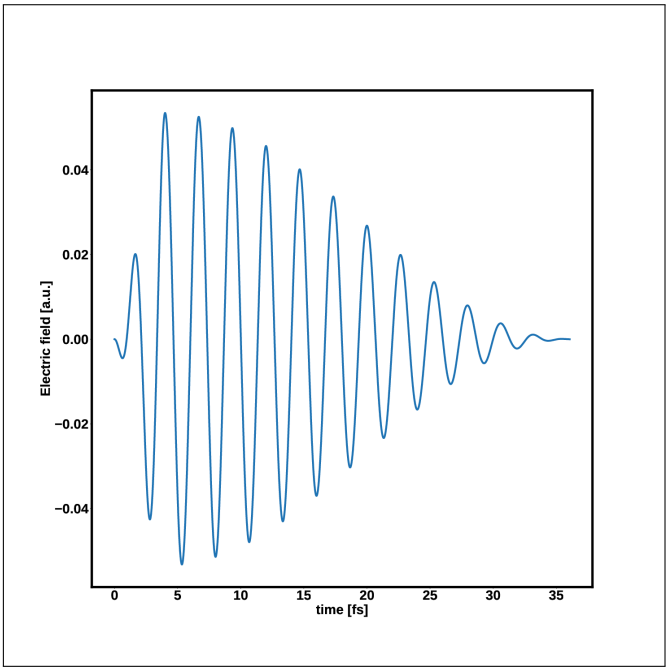

Fig. S1. Simulating ionic response after strong-field ionization. The electric field of the pump acting on the ion is ramped-up smoothly over 1.5 cycles (≈ 4 fs) from zero to the peak electric field strength at the time of ionization. This eliminates possible artefacts associated with populating field-free ionic states at the maximum of the electric field.

with the reduced mass of N_2^+, μ, and using the potential energy curves of the electronic states X, A, and B from Refs. [6, 7], where the potential energy curve of B is shifted by $\delta E = 0.00188$ a.u. to reproduce the experimental value of the energy gap $\Delta E = E_{B0} - E_{X0} \approx 3.17$ eV ($\lambda \approx 391$ nm).

We then solve the following system of coupled equations,

$$i\frac{d}{dt}\,a_{n\nu}^{(n_0\nu_0)}(t;\theta) = E_{n\nu}a_{n\nu}^{(n_0\nu_0)}(t;\theta) - \sum_{n'\nu'} F_{\mathrm{pu}}(t)D_{n\nu,n'\nu'}(\theta)\,a_{n'\nu'}^{(n_0\nu_0)}(t;\theta)\,, \tag{S4}$$

for several fixed values of θ, ranging from 0 to π with $\Delta\theta = \pi/64 \approx 0.05$, using the Runge-Kutta method with a time step of $\Delta t = 0.01$ a.u. ($\Delta t \approx 0.0002$ fs).

The superscript $(n_0\nu_0)$ of the amplitudes indicates the initial vibronic state. We initialize dynamics in the X state and in the B state, starting from both the ground and first excited vibrational level, respectively. The two sets of vibronic amplitudes obtained at the end of the propagation calculations, which started in the same electronic state but different vibrational levels, are summed and weighted with the corresponding Franck-Condon factors (see Eq. (S8) below).

The molecular transition dipole operator is given by

$$\begin{aligned} D_{n\nu,n'\nu'}(\theta) &= g_{n,n'}(\theta)\,d_{n\nu,n'\nu'} \\ &= g_{n,n'}(\theta)\int dR\;\psi_{n\nu}^*(R)d_{n,n'}(R)\psi_{n'\nu'}(R), \end{aligned} \tag{S5}$$

where $d_{n,n'}(R)$ is the transition dipole element between the two electronic states n and n' of N_2^+ as a function of the internuclear distance R, and taken from Refs. [6, 7]. $g_{n,n'} = \cos(\theta)$ for the parallel dipole coupling between the states X and B, $g_{n,n'} =$

$\sin(\theta)$ for the perpendicular dipole coupling between the states X and A, and $g_{n,n'} = 0$ otherwise.

4. FIELD-FREE EVOLUTION OF N_2^+ AFTER THE PUMP

After the end of the pump pulse ($t > T_{\rm pu}$), the field-free evolution of the rotational wave packet created in the ground vibrational level $\nu = 0$ in the electronic state X, starting from a pure rotational eigenstate $|J_0M_0\rangle$ and the ion initially produced in the X state, is described by

$$|\Psi_{X0}^{(XJ_0M_0)}(t)\rangle = \sum_J a_{X0J}^{(XJ_0M_0)}(T_{\rm pu}) e^{-iE_{X0J}(t-T_{\rm pu})}|JM_0\rangle, \quad \text{(S6)}$$

where

$$a_{X0J}^{(X,J_0,M_0)}(T_{\rm pu}) = \langle JM_0|\tilde{a}_{X0}^{(X)}(\theta, T_{\rm pu}, t_{\rm ion})|J_0M_0\rangle_{\theta,\phi} \quad \text{(S7)}$$

and

$$\tilde{a}_{X0}^{(X)}(\theta, T_{\rm pu}, t_{\rm ion}) = \sqrt{r_X w(\theta)}\left(c_{X0}^{\rm FC} a_{X0}^{(X0)}(T_{\rm pu};\theta) + c_{X1}^{\rm FC} a_{X0}^{(X1)}(T_{\rm pu};\theta)\right) e^{-i\Phi_N(\theta;t_{\rm ion})} \quad . \quad \text{(S8)}$$

For convenience, in Eqs. (S6), (S7) and below we omit to denote the parametric $t_{\rm ion}$-dependence of the amplitude $a_{X0J}^{(X,J_0,M_0)}$.

The ket $|JM_0\rangle$ labels the field-free rotational state (given by the spherical harmonic $Y_{JM_0}(\theta,\phi)$ for Σ electronic states) with quantum numbers J and M_0, where $J = 0,\ldots,59$ and $M_0 = -J,-(J-1),\ldots,(J-1),J$ (note that $M = M_0$ is conserved in a linearly polarized field). The energy, E_{X0J}, is given by $E_{X0J} = E_{X0} + B_X^0 J(J+1)$, where $B_X^0 = 1.93176\ \text{cm}^{-1}$ is the rotational constant of state X of N_2^+.

Assuming a vertical promotion (Franck–Condon excitation) of the nuclear wave function from the vibrational ground level of the electronic ground state of N_2 into the corresponding vibronic state of the ion, the Franck-Condon factors are given by $c_{X0}^{\rm FC} \approx 0.9369$ and $c_{X1}^{\rm FC} \approx 0.3348$. The electronic ground state of N_2 is calculated using a Morse potential based on parameters taken from the NIST Webbook [8] and optimized against experimental photoelectron spectra [9]. The optimized equilibrium bond length is found to be $R_e = 1.1033$ Å. The ionization rate factor for X is set to $r_X = 1.0$.

The field-free evolution of the rotational wave packet,

$$|\Psi_{B0}^{(BJ_0M_0)}(t)\rangle = \sum_J a_{B0J}^{(BJ_0M_0)}(T_{\rm pu}) e^{-iE_{B0J}(t-T_{\rm pu})}|JM_0\rangle, \quad \text{(S9)}$$

created in the ground vibrational level $\nu = 0$ in the electronic state B, starting from the pure rotational eigenstate $|J_0M_0\rangle$ and associated with ionization into B, is defined analogously to Eqs. (S6)-(S8), but using the energy $E_{B0J} = E_{B0} + B_B^0 J(J+1)$ (with $B_B^0 = 2.07456\ \text{cm}^{-1}$), the amplitudes $a_{B0}^{(B0)}(T_{\rm pu};\theta)$ and $a_{B0}^{(B1)}(T_{\rm pu};\theta)$ multiplied by the respective Franck-Condon factors $c_{B0}^{\rm FC} \approx 0.9589$ and $c_{B1}^{\rm FC} \approx -0.2823$, and the ionization rate factor $r_B = 0.2$.

5. ENSEMBLE-AVERAGED MOLECULAR ALIGNMENT

After the pump pulse ($t > T_{\rm pu}$), during the field-free propagation, molecular alignment is characterized by the expectation value $\langle\cos^2\theta\rangle$. For the rotational wave packet in Eq. (S6), the population-weighted alignment measure is given by

$$P_X^{(XJ_0M_0)}\langle\cos^2\theta\rangle_X^{(XJ_0M_0)}(t) = \langle\Psi_{X0}^{(XJ_0M_0)}(t)|\cos^2\theta|\Psi_{X0}^{(XJ_0M_0)}(t)\rangle$$
$$= \sum_J \Big[\, |a_{X0J}|^2\left(C_{J,J+1}^2 + C_{J,J-1}^2\right) + 2|a_{X0J}||a_{X0J+2}| \times$$
$$\times C_{J,J+1}C_{J+1,J+2}\cos\left(\omega_{J+2,J}^{XX}t + \phi_X^0(J,J+2)\right)\Big], \quad \text{(S10)}$$

Here, the amplitudes $a_{X0J'}$ are those obtained at the end of the pump pulse ($t = T_{\rm pu}$), where we have omitted their common superscript, (XJ_0M_0), cf. Eq. (S6). The matrix element $C_{J,J'}$ is given by $C_{J,J'} = \langle JM_0|\cos\theta|J'M_0\rangle$, the frequency $\omega_{J+2,J}^{XX} = E_{X0J+2} - E_{X0J}$, and $\phi_X^0(J,J+2)$ is the phase difference between the states $|X0,JM_0\rangle$ and $|X0,J+2M_0\rangle$ at $t = T_{\rm pu}$.

The alignment measure of the rotational wave packet created in the $|B0\rangle$ state, $P_B^{(BJ_0M_0)}\langle\cos^2\theta\rangle_B^{(BJ_0M_0)}(t)$, is given by an expression analogue to Eq. (S10), using the rotational wave packet $|\Psi_{B0}^{(BJ_0M_0)}(t)\rangle$ defined in Eq. (S9).

The alignment measure is thermally averaged by adding the contributions of the rotational wave packets originating from each rotational state $|J_0M_0\rangle$ in the initial Boltzmann distribution incoherently, each weighted by the corresponding Boltzmann probability, $w_{J_0} = \exp(-B_N^0 J_0(J_0+1)/k_{\rm B}T)$, where $k_{\rm B}$ is the Boltzmann constant and $B_N^0 = 1.989581\ \text{cm}^{-1}$ is the rotational constant of the ground state of N_2, and multiplied by the nuclear spin statistics factor g_J. The relative weight, g_J, of even and odd J is 2:1 for the X state and 1:2 for the B state.

6. GAIN-LOSS CALCULATIONS

To obtain the frequency-resolved gain and loss shown in Figs. 2(a) and 3(a,b) of the main article, we apply conventional transient absorption theory [10–12] and calculate the linear response of the pumped system to a weak, time-delayed laser pulse. The energy exchanged between the pumped system and the electric field of the probe pulse, $F_{\rm pr}(t)$, is given by

$$\Delta\mathcal{E} = -\int_{-\infty}^{+\infty} dt\, d^{(1)}(t)\,\frac{\partial F_{\rm pr}(t)}{\partial t}\,, \quad \text{(S11)}$$

where $d^{(1)}(t)$ is the probe-induced dipole in the pumped system to first order with respect to the probe pulse.

Linear transient absorption at the frequencies

$$\omega_{J,J-1}^{BX} = E_{B0J} - E_{X0J-1}, \quad \text{(S12)}$$
$$\omega_{J,J+1}^{BX} = E_{B0J} - E_{X0J+1}, \quad \text{(S13)}$$

stimulated by a short, weak Gaussian probe pulse with a time delay $\tau > 0$ with respect to the pump pulse, is described by

$$\Delta\mathcal{E}_J^{(XJ_0M_0)}(\omega_{J,J-1}^{BX},\omega_{J,J+1}^{BX},\tau) = \omega_{\rm pr}|F_{0,\rm pr}|^2|d_{X0,B0}|^2 4\pi^2 \times$$
$$\times\Big[\;\; |a_{X0J+1}|^2\, C_{J,J+1}^2\, |\tilde{f}_{\rm pr}(\Delta\omega_{J,J+1}^{BX})|^2 +$$
$$+|a_{X0J-1}|^2\, C_{J,J-1}^2\, |\tilde{f}_{\rm pr}(\Delta\omega_{J,J-1}^{BX})|^2 +$$
$$+2|a_{X0J+1}||a_{X0J-1}|C_{J,J+1}C_{J,J-1}\tilde{f}_{\rm pr}^*(\Delta\omega_{J,J+1}^{BX})\tilde{f}_{\rm pr}(\Delta\omega_{J,J-1}^{BX}) \times$$
$$\times\cos\left(\omega_{J+1,J-1}^{XX}\tau + \phi_X^0(J-1,J+1)\right)\Big]. \quad \text{(S14)}$$

In Eq. (S14), we again have omitted the $T_{\rm pu}$-dependence and the common superscript (XJ_0M_0) of all amplitudes $a_{X0J'}$.

The probe pulse is defined by $F_{\rm pr}(t) = F_{0,\rm pr} f_{\rm pr}(t-\tau)\exp(-i\omega_{\rm pr}t) + c.c.$, with the peak field strength $F_{0,\rm pr} = 0.00169$ a.u. (or peak intensity $I_{0,\rm pr} = 10^{11}$ W/cm^2), the carrier frequency $\omega_{\rm pr} = 0.1165$ a.u. (or carrier wavelength $\lambda_{\rm pr} = 391$ nm), and a Gaussian envelope $f_{\rm pr}(t-\tau)$ with a full width at half maximum of 20 fs in intensity. $\tilde{f}_{\rm pr}(\Delta\omega^{BX}_{J,J'})$ denotes the Fourier transform of the Gaussian envelope of the probe pulse at frequency $\Delta\omega^{BX}_{J,J'} = \omega^{BX}_{J,J'} - \omega_{\rm pr}$. Our Fourier transform convention is $g(t) = \int_{-\infty}^{\infty} \tilde{g}(\omega)\exp(-i\omega t)\,d\omega$ and $\tilde{g}(\omega) = 1/(2\pi)\int_{-\infty}^{\infty} g(t)\exp(i\omega t)\,dt$. $\phi^0_X(J-1,J+1)$ denotes the phase difference between the states $|X0,J-1M_0\rangle$ and $|X0,J+1M_0\rangle$ at the end of the pump pulse ($t = T_{\rm pu}$).

The first two terms in Eq. (S14) correspond to absorption at the frequencies associated with the lower-energy P-branch ($\omega^{BX}_{J,J+1}$) and the higher-energy R-branch ($\omega^{BX}_{J,J-1}$) of the $B(\nu=0) \leftarrow X(\nu=0)$ absorption spectrum, respectively. The third term describes the interference between the two absorption paths associated with the two branches that lead to the same final state $|B0,JM_0>$, i.e., the interference between the two transitions $|B0,JM_0\rangle \leftarrow |X0,J-1M_0\rangle$ and $|B0,JM_0\rangle \leftarrow |X0,J+1M_0\rangle$.

Linear transient emission (negative absorption) at the frequencies

$$|\omega^{XB}_{J,J-1}| = |E_{X0J} - E_{B0J-1}|, \tag{S15}$$

$$|\omega^{XB}_{J,J+1}| = |E_{X0J} - E_{B0J+1}|, \tag{S16}$$

stimulated by the same time-delayed probe pulse, is described analogously to Eq. (S14), but includes the amplitudes and initial phases of the states $|B0,J-1M_0\rangle$ and $|B0,J+1M_0\rangle$:

$$\begin{aligned}\Delta\mathcal{E}_J^{(BJ_0M_0)}(|\omega^{XB}_{J,J-1}|,|\omega^{XB}_{J,J+1}|,\tau) = -\omega_{\rm pr}|F_{0,\rm pr}|^2|d_{X0,B0}|^2 4\pi^2\times\\ \times\Big[\ |a_{B0J+1}|^2\,C^2_{J,J+1}\,|\tilde{f}_{\rm pr}(\Delta\omega^{XB}_{J,J+1})|^2+\\ +|a_{B0J-1}|^2\,C^2_{J,J-1}\,|\tilde{f}_{\rm pr}(\Delta\omega^{XB}_{J,J-1})|^2+\\ +2|a_{B0J+1}||a_{B0J-1}|C_{J,J+1}C_{J,J-1}\tilde{f}^*_{\rm pr}(\Delta\omega^{XB}_{J,J+1})\tilde{f}_{\rm pr}(\Delta\omega^{XB}_{J,J-1})\times\\ \times\cos\left(\omega^{BB}_{J+1,J-1}\tau+\phi^0_B(J-1,J+1)\right)\Big].\end{aligned} \tag{S17}$$

The $T_{\rm pu}$-dependence and the common superscript (BJ_0M_0) of all amplitudes $a_{B0J'}$ are omitted again. Analog to Eq. (S14), the first two terms in Eq. (S17) describe emission at the frequencies associated with the R and P branches of the $X(\nu=0) \leftarrow B(\nu=0)$ emission spectrum, respectively. The third term describes the interference between the two emission paths associated with the two branches that lead to the same final state $|X0,JM_0>$.

Let $W_{\rm abs}(\tau) = \langle\sum_J \Delta\mathcal{E}_J^{(XJ_0M0)}\rangle_{J_0,M_0}(\tau)$ be the ensemble-averaged, frequency-integrated transient absorption probability, where the ensemble average of the transient absorption signal is calculated analogously to the ensemble-averaged alignment measure. Note that for $\tilde{f}_{\rm pr}(\Delta\omega^{\rm BX}_{J,J-1}) \simeq \tilde{f}_{\rm pr}(\Delta\omega^{\rm BX}_{J,J+1})$, we find that $W_{\rm abs}(\tau) \propto P_X\langle\cos^2\theta\rangle_X(\tau)$, where $\langle\cos^2\theta\rangle_X(\tau)$ is the ensemble-averaged alignment measure of state X and P_X its population.

The alignment measure of the rotational wave packet created in the $|B0\rangle$ state, $P_B^{(BJ_0M_0)}\langle\cos^2\theta\rangle_B^{(BJ_0M_0)}(t)$, is given by an expression analogue to Eq. (S10). Thus, for $\tilde{f}_{\rm pr}(\Delta\omega^{\rm XB}_{J,J-1}) \simeq \tilde{f}_{\rm pr}(\Delta\omega^{\rm XB}_{J,J+1})$, we find that $W_{\rm em}(\tau) \propto P_B\langle\cos^2\theta\rangle_B(\tau)$, where $W_{\rm em}(\tau) = \langle\sum_J \Delta\mathcal{E}_J^{(BJ_0M0)}\rangle_{J_0,M_0}(\tau)$ is the ensemble-averaged, frequency-integrated transient emission probability and $P_B\langle\cos^2\theta\rangle_B(\tau)$ is the ensemble-averaged alignment measure of state B with population P_B.

7. DEPENDENCE OF GAIN ON THE PUMP INTENSITY

In Fig. S2(a), we show the gain obtained at the pump-probe delay $\tau_1 \simeq 4.4$ ps (corresponding to the first distinct gain window in Fig. 2(d) of the main article) as a function of the peak intensity of the pump pulse, ranging from 5×10^{13} W/cm^2 to 4×10^{14} W/cm^2. Our theoretical modeling has limitations at very high intensities: we only include three potential energy surfaces of the N_2^+ ion and neglect molecular rotations during the pulse. At intensities of $3-4\times10^{14}$ W/cm^2 and above these approximations will start to fail. Nevertheless, the improvement of gain with increasing intensity above 3×10^{14} W/cm^2 is realistic. For the sake of clarity, we have only varied the peak intensity of the pump, keeping all other parameters the same as in Fig. 2 of the main article. For the highest peak intensities, ionization is expected to take place before the peak of the pulse envelope, during the turn-on, which is not considered in Fig. S2.

The intensity-dependent gain shown in orange is obtained by calculating the frequency- and delay-dependent transient absorption signal for a given peak intensity of the pump, integrating the signal over all frequencies (analog to the gain-loss balance shown in green in Fig. 2(d) of the main article for $I_{0,\rm pu} = 1\times10^{14}$ W/cm^2), and determining the optimum delay around $\tau_1 = 4.4$ ps. Around this delay, pronounced gain windows similar to the one in Fig. 2(d) of the main article emerge for all pump intensities, with the optimum delay varying by a few tens of femtoseconds. The gain shown in violet and fuchsia is found analogously, except that before frequency integration the transient absorption signal was multiplied by the violet and fuchsia frequency-window masks (bins) indicated in Fig. S2(c), respectively.

In all three cases, the gain increases with intensity up to $I_{0,\rm pu} = 1\times10^{14}$ W/cm^2, where it starts to drop until $I_{0,\rm pu} = 2\times10^{14}$ W/cm^2, followed by another rise.

In Fig. S2(b), we show the gain at $\tau_1 \simeq 4.4$ ps after integrating over a radial Gaussian intensity distribution of the pump pulse, re-normalized to the averaged gain at the highest intensity. Considering volume averaging for the case of loose focussing in a low-density gas, we obtain very similar results. The averaged gain increases monotonically, with the intensity-dependent modulations smoothed out.

In the recent work of Ref. [13], the dependence of the peak pulse intensity on the pressure in air has been determined for a wide range of pressures. Comparison with the results in Ref. [13] suggests that, with inhomogeneous intensity distribution included in the analysis, the optimal pressure regime may be well below 1 bar.

REFERENCES

1. T. Seideman, "On the dynamics of rotationally broad, spatially aligned wave packets," The J. Chem. Phys. **115**, 5965–5973 (2001).
2. M. Spanner and S. Patchkovskii, "One-electron ionization of multielectron systems in strong nonresonant laser fields," Phys. Rev. A **80**, 063411 (2009).

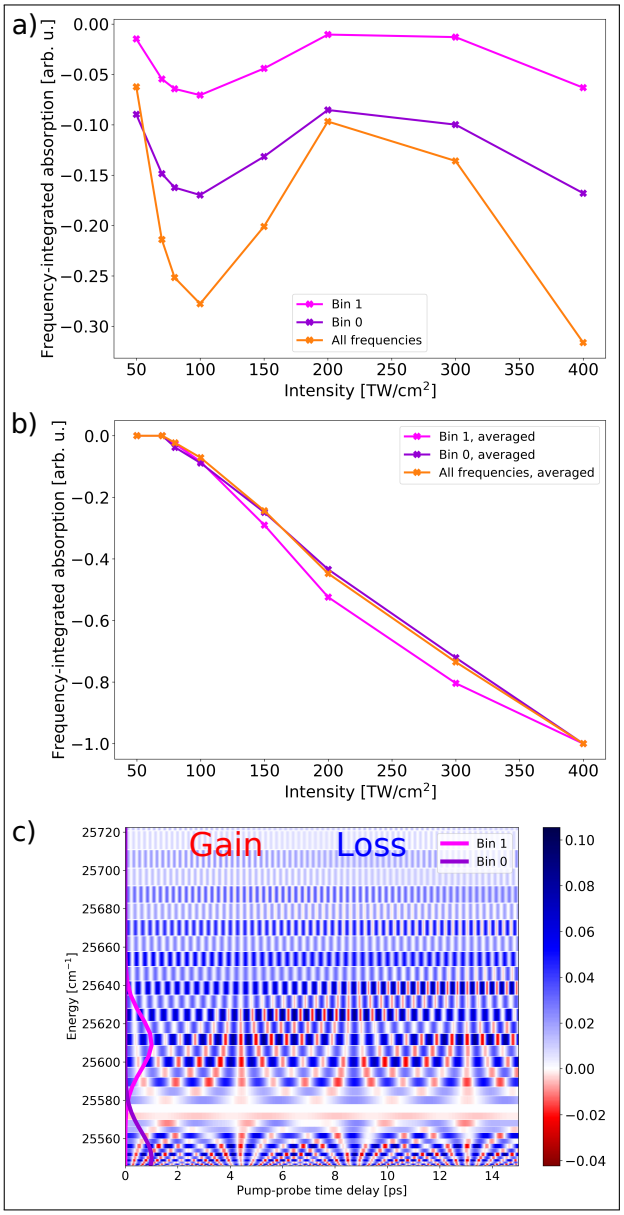

Fig. S2. Dependence of gain at the pump-probe time delay $\tau_1 \simeq 4.4$ ps (corresponding to the first distinct gain window in Fig. 2(d) of the main article) on the peak pump intensity. All parameters except the pump intensity are kept the same as in Fig. 2 of the main article. (a) Gain at $\tau_1 \simeq 4.4$ ps obtained by integration of the transient absorption signal over all frequencies (orange), and by frequency integration of the transient absorption signal multiplied by the violet (violet) and fuchsia (fuchsia) frequency-window masks (bins) indicated in panel (c). (b) Gain at $\tau_1 \simeq 4.4$ ps, after integrating over the inhomogeneous radial intensity distribution of the pump, re-normalized to the averaged gain at the highest intensity. (c) Frequency-resolved gain (red) and loss (blue) of the weak probe interacting with the pumped system as a function of pump-probe time delay for a pump intensity of $I_{0,\mathrm{pu}} = 8 \times 10^{13}$ W/cm^2.

3. M. Spanner and S. Patchkovskii, "Molecular strong field ionization and high harmonic generation: A selection of computational illustrations," Chem. Phys. **414**, 10 – 19 (2013).
4. M. W. Schmidt, K. K. Baldridge, J. A. Boatz, S. T. Elbert, M. S. Gordon, J. H. Jensen, S. Koseki, N. Matsunaga, K. A. Nguyen, S. Su, T. L. Windus, M. Dupuis, and J. A. Montgomery Jr, "General atomic and molecular electronic structure system," J. Comput. Chem. **14**, 1347–1363 (1993).
5. D. E. Manolopoulos, "Derivation and reflection properties of a transmission-free absorbing potential," The J. Chem. Phys. **117**, 9552–9559 (2002).
6. S. R. Langhoff, C. W. Bauschlicher, and H. Partridge, "Theoretical study of the N_2^+ Meinel system," The J. Chem. Phys. **87**, 4716–4721 (1987).
7. S. R. Langhoff and C. W. Bauschlicher, "Theoretical study of the first and second negative systems of N_2^+," The J. Chem. Phys. **88**, 329–336 (1988).
8. "Nist chemistry webbook: https://webbook.nist.gov/cgi/cbook.cgi?ID=C7727379&Mask=1000#Diatomic," (2019).
9. K. Kimura, S. Katsumata, Y. Achiba, T. Yamazaki, and S. Iwata, *Handbook of HeI photoelectron spectra of fundamental organic molecules: ionization energies, ab initio assignments, and valence electronic structure for 200 molecules* (Japan Scientific Societies Press, Tokyo und Halstead Press, New York, 1981).
10. W. T. Pollard, S. Lee, and R. A. Mathies, "Wave packet theory of dynamic absorption spectra in femtosecond pump–probe experiments," The J. Chem. Phys. **92**, 4012–4029 (1990).
11. R. Santra, V. S. Yakovlev, T. Pfeifer, and Z.-H. Loh, "Theory of attosecond transient absorption spectroscopy of strong-field-generated ions," Phys. Rev. A **83**, 033405 (2011).
12. M. Wu, S. Chen, S. Camp, K. J. Schafer, and M. B. Gaarde, "Theory of strong-field attosecond transient absorption," J. Phys. B: At. Mol. Opt. Phys. **49**, 062003 (2016).
13. P. M. Solyankin, I. A. Nikolaeva, A. A. Angeluts, D. E. Shipilo, N. V. Minaev, N. A. Panov, A. V. Balakin, Y. Zhu, O. G. Kosareva, and A. P. Shkurinov, "THz generation from laser-induced breakdown in pressurized molecular gases: on the way to terahertz remote sensing of the atmospheres of Mars and Venus," New J. Phys. **22**, 013039 (2020).